

Feasibility of developing an ionospheric E-region electron density storm model using TIMED/SABER measurements

J.R. Fernandez^a, C.J. Mertens^{a,*}, D. Bilitza^b, X. Xu^c, J.M. Russell III^d, M.G. Mlynczak^a

^a NASA Langley Research Center, Hampton, VA, USA

^b George Mason University, Fairfax, VA, USA

^c SSAI, Inc., Hampton, VA, USA

^d Hampton University, Hampton, VA, USA

Received 23 January 2009; received in revised form 9 September 2009; accepted 20 November 2009

Abstract

We present a new technique for improving ionospheric models of nighttime E-region electron densities under geomagnetic storm conditions using TIMED/SABER measurements of broadband 4.3 μm limb radiance. The response of E-region electron densities to geomagnetic activity is characterized by SABER-derived $\text{NO}^+(\text{v})$ 4.3 μm Volume Emission Rates (VER). A storm-time E-region electron density correction factor is defined as the ratio of storm-enhanced $\text{NO}^+(\text{v})$ VER to a quiet-time climatological average $\text{NO}^+(\text{v})$ VER, which will be fit to a geomagnetic activity index in a future work. The purpose of this paper is to demonstrate the feasibility of our technique in two ways. One, we compare storm-to-quiet ratios of SABER-derived $\text{NO}^+(\text{v})$ VER with storm-to-quiet ratios of electron densities measured by Incoherent Scatter Radar. Two, we demonstrate that $\text{NO}^+(\text{v})$ VER can be parameterized by widely available geomagnetic activity indices. The storm-time correction derived from $\text{NO}^+(\text{v})$ VER is applicable at high-latitudes.

Published by Elsevier Ltd. on behalf of COSPAR.

Keywords: Infrared remote sensing; Ionosphere; E-region; Magnetic storm; SABER

1. Introduction

The Sounding of the Atmosphere using Broadband Emission Radiometry (SABER) instrument is a multi-channel radiometer onboard the Thermosphere–Ionosphere–Mesosphere–Energetics and Dynamics (TIMED) satellite (Russell et al., 1999). TIMED was launched in December, 2001. Continuous SABER measurements began in January 2002. SABER scans the Earth's limb line-of-sight and radiance measurements are made by 10 broadband radiometer channels from 1.27 to 17 μm . Depending on the specific data product, geophysical parameters are derived at tangent altitudes ranging from the tropopause to over 180 km. Daytime and nighttime measurements are made over a latitude range

that alternates hemispheres in a 60-day yaw period, extending in latitude from 83° in one hemisphere to 52° in the opposite hemisphere. After approximately 60 days, the TIMED satellite performs a yaw maneuver and the hemispheric coverage is reversed, as depicted in Fig. 1. Dashed lines in Fig. 1 indicate dates of the yaw maneuvers for the year 2003. Similar yaw dates are performed every year. The SABER quiet-time climatological averages discussed in Section 2 are multi-year (2002–2006), quasi-seasonal averages based on the SABER yaw cycles shown in Fig. 1. Hemispheric symmetry is also assumed in the data analysis.

Radiance measurements at 4.3 μm are significantly increased during geomagnetic disturbances, such as during the Halloween 2003 superstorm reported by Mertens et al. (2007a). These enhancements are due to vibrationally excited NO^+ emissions produced by precipitating auroral electrons that increase the ionization of the neutral atmosphere. At E-region altitudes, these ions react with neutral

* Corresponding author.

E-mail address: c.j.mertens@larc.nasa.gov (C.J. Mertens).

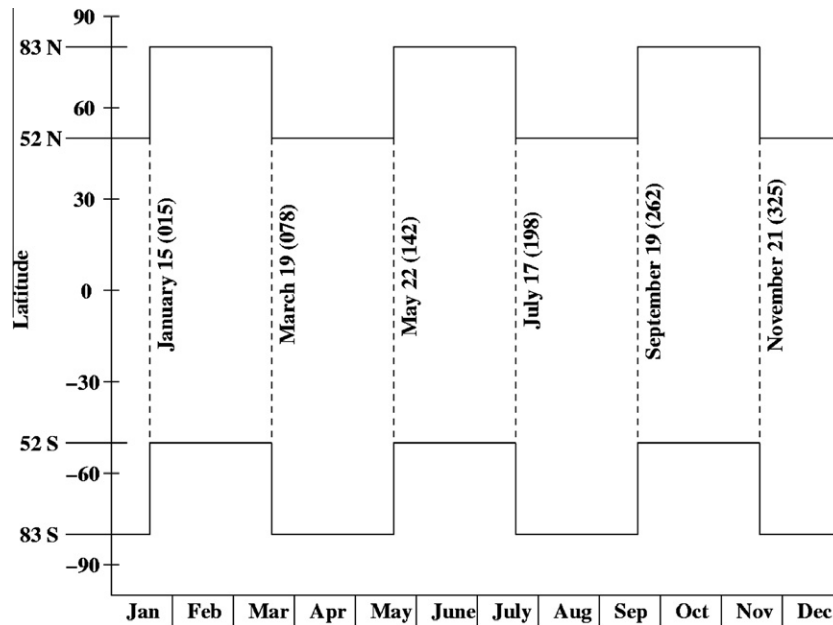


Fig. 1. TIMED/SABER latitude coverage during 2003. Dashed line indicates the yaw maneuvers.

species to produce NO^+ (Torr et al., 1990; Fox and Sung, 2001). Moreover, some of these reactions are exothermic enough to produce $\text{NO}^+(\nu)$, which emits at $4.3 \mu\text{m}$. In order to isolate the $\text{NO}^+(\nu)$ emissions, a new $\text{NO}^+(\nu)$ Volume Emission Rate (VER) data product was produced by simulating the $\text{CO}_2(\nu_3)$ contribution and subtracting it from the measured radiance values using non-local thermodynamic equilibrium (non-LTE) algorithms, and performing a standard Abel inversion on the residual radiance. This procedure is applied to nighttime $4.3 \mu\text{m}$ measurements since $\text{CO}_2(\nu_3)$ contributions are dominant during daytime. The error in modeling the $\text{CO}_2(\nu_3)$ contribution is on the order of 20%. During modest geomagnetic storms, the $\text{NO}^+(\nu)$ emission contributes 60–80% of the $4.3 \mu\text{m}$ limb radiance measured by SABER. Thus, the SABER-derived storm-time $\text{NO}^+(\nu)$ VER modeling error is expected to be on the order of 4–8% for moderate geomagnetic storms with decreasing errors for stronger storms (Mertens et al., 2007a).

There are other sources of uncertainty associated with deriving the $\text{NO}^+(\nu)$ VER from a 1D Abel inversion. The uncertainties are due to affects of non-tangent layer emission and non-homogeneous, horizontal spatial structure in NO^+ along the limb line-of-sight. These influences are difficult to assess and can induce biases and non-physical vertical structure in the derived single-profile VER. However, it is reasonable to expect that these errors will be partially filtered out in developing the storm-time correction model by computing altitude averages (see Section 2) and by binning the $\text{NO}^+(\nu)$ VER in latitude bands and according to geomagnetic activity indices (Mertens et al., 2009b). The most reliable assessment of errors in the approach is to conduct numerous comparisons with independent measurements such as presented in Section 4 and by Mertens et al. (2009b).

Fig. 2 shows an example of both radiance and SABER-derived $\text{NO}^+(\nu)$ VER at 60N and 227E for two measurement scans: before (blue line) and during (red line) the Halloween 2003 magnetic storm. Note that at quiet times, radiances values reach the $4.3 \mu\text{m}$ channel detector noise limit, denoted by the Noise Equivalent Radiance (NER), at about 135 km. During the geomagnetically disturbed periods, the $4.3 \mu\text{m}$ limb radiance measurements do not reach the noise limit until above 180 km. Storm-enhanced radiances are increased by several orders of magnitude compared to quiescent values. VER values are also enhanced as shown in the right panel.

$\text{NO}^+(\nu)$ VER enhancements can be used as a proxy to characterize the electron density during geomagnetic storms at high-latitudes since the $\text{NO}^+(\nu)$ VER enhancements are mainly due to auroral particle precipitation (Mertens et al., 2007a,b). The global $\text{NO}^+(\nu)$ VER distribution, near the altitude of the E-region electron density peak, correlates very well with patterns of auroral particle precipitation measured by the NOAA/POES satellites (Mertens et al., 2009a, 2007b). This led to the idea of using a storm-to-quiet time ratio (SQR) to generate a correction factor for the International Reference Ionosphere (IRI) model. The IRI model is an empirical model widely used in the ionospheric community to obtain climatological mean values for the electron density, electron and ion temperatures, among other parameters (Bilitza, 2001). However, parameterizations in IRI for geomagnetic storm activity remain largely incomplete, and there is currently no storm-time correction to IRI parameters in the E-region. In this work, we demonstrate the feasibility of using the SABER $\text{NO}^+(\nu)$ VER SQR to develop a storm-time E-region electron density correction factor by comparing with Incoherent Scatter Radar (ISR) measurements for several geomagnetic storm events.

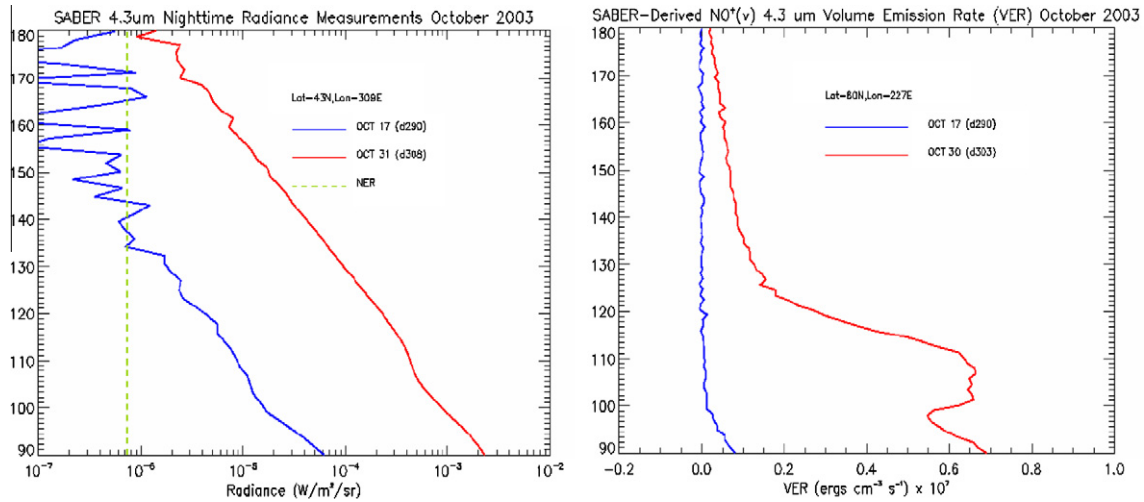


Fig. 2. Nighttime radiance and VER measurements before (blue line) and during (red line) Halloween 2003 magnetic storm. (For interpretation of the references to color in this figure legend, the reader is referred to the web version of this paper.)

In a future work, the SABER $\text{NO}^+(\nu)$ VER SQR will form the basis for an empirical correction to E-region electron densities during geomagnetic disturbances, and applied to the IRI, as briefly described in Section 2. In order to develop the empirical correction, we will derive a parametric relation between SABER $\text{NO}^+(\nu)$ VER SQR and an appropriate geomagnetic index. In order to select an appropriate index, we derive the cross-correlation function between SABER $\text{NO}^+(\nu)$ VER and the most common and widely used geomagnetic indices. The cross-correlation functions are computed for the Halloween 2003 storm period, which are presented in Section 3. In Section 4, we show SQR comparisons between ISR and SABER $\text{NO}^+(\nu)$ VER for different storm events and ISR locations. Our conclusions are given in Section 5.

2. Storm-time correction model

SABER-derived $\text{NO}^+(\nu)$ VER provides a new tool for monitoring the nighttime ionosphere during geomagnetic storm-time periods. By computing storm-to-quiet ratios, they can be used as a proxy to estimate the electron density enhancements at E-region altitudes. Thus, $\text{NO}^+(\nu)$ VER SQR values denoted by r are defined by

$$r(z, \lambda_m, \varphi_m, t) = \frac{\text{VER}_{\text{Storm}}(z, \lambda_m, \varphi_m, t)}{\text{VER}_{\text{Quiet}}(z, \lambda_m, \varphi_m)}, \quad (1)$$

where z , t , λ_m , and φ_m are altitude, UT time, magnetic latitude, and magnetic longitude (or magnetic local time), respectively. The quiet-time $\text{NO}^+(\nu)$ VER are time independent, by definition, since they represent a climatological average over a period of geomagnetic undisturbed conditions. The reason for introducing the ratio in (1) is the observation that

$$r \approx \frac{[\text{NO}^+]_{\text{Storm}}}{[\text{NO}^+]_{\text{Quiet}}} \approx \frac{[e]_{\text{Storm}}}{[e]_{\text{Quiet}}}, \quad (2)$$

where $[e]$ is the electron density. There are two primary assumptions implied in (1) and (2). The first assumption is that the $\text{NO}^+(\nu)$ VER storm-to-quiet ratio is approximately equal to the storm-to-quiet ratio of NO^+ density. This assumption is justifiable because the dominate ion-neutral chemical reactions responsible for the production of NO^+ are also the same ones exothermic enough to vibrationally excite the NO^+ states that emit in the 4.3 μm spectral region. The second assumption is that the storm-to-quiet ratio of NO^+ density is approximately equal to the electron density storm-to-quiet ratio. This assumption is justifiable since NO^+ is the terminal E-region ion. Thus, (1) and (2) describe the fundamental basis of our storm-time E-region electron density correction, of which we demonstrate the feasibility in this work.

The $\text{NO}^+(\nu)$ VER SQR is a finite, well-behaved quantity, even outside the auroral oval region. The $\text{NO}^+(\nu)$ VER is derived by performing an Abel inversion on the residual radiance, i.e., the measured radiance minus $\text{CO}_2(\nu_3)$ contribution. The Abel integral equation is classified as a Fredholm integral equation of the first kind. A unique, stable numerical inversion is obtained by employing Philips–Tikhonov–Twomey (PTT) regularization (Philips, 1962; Tikhonov, 1963; Twomey, 1963, 1977). Our optimized PTT-regularization approach matches the simulated and measured 4.3 μm limb radiance to within the SABER detector noise and ensures the first derivatives in the $\text{NO}^+(\nu)$ VER are continuous. The 4.3 μm channel NER is $7.35 \times 10^{-7} \text{ W m}^{-2} \text{ sr}^{-1}$, which maps into a VER of $\sim 2 \times 10^{-9} \text{ ergs cm}^{-3} \text{ s}^{-1}$. This guarantees that the denominator in (1) is finite. Thus, under geomagnetically quiet conditions, $r \sim 1$ at all latitudes.

The robustness of the $\text{NO}^+(\nu)$ VER SQR is illustrated in Fig. 3. This figure shows global distributions of time-averaged $\text{NO}^+(\nu)$ VER for the quasi-seasonal period overlapping the Halloween 2003 superstorm. The left panel shows the climatological quiet-time $\text{NO}^+(\nu)$ VER, which

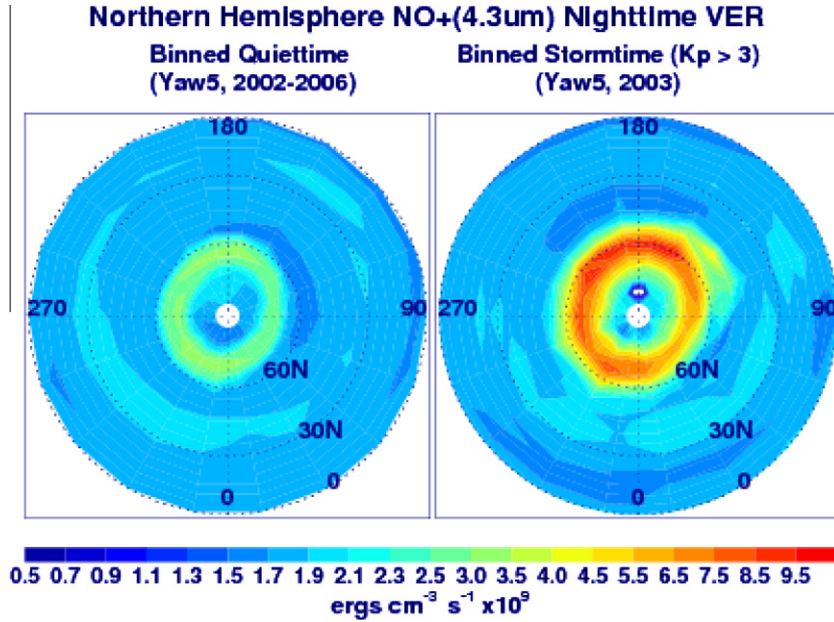


Fig. 3. Global distribution of (left) quiet-time climatological $\text{NO}^+(\text{v})$ VER and (right) storm-time $\text{NO}^+(\text{v})$ VER. In both panels, the VER were altitude averaged from 116 to 120 km. The quiet-time ($kp \leq 3$) VER were time-averaged over September–November for years 2002–2006. The storm-time ($kp > 3$) VER were time-averaged over September–November in year 2003.

is used in the denominator in (1) to calculate our E-region electron density storm-time correction factor. Note that there is still a small level of enhanced $\text{NO}^+(\text{v})$ VER during our defined quiet-time ($kp \leq 3$) in the auroral oval region. However, it is the relative storm-to-quiet $\text{NO}^+(\text{v})$ VER that is utilized in developing the E-region electron density storm-time correction. For comparison, the right panel shows geomagnetically disturbed ($kp > 3$) $\text{NO}^+(\text{v})$ VER averaged over September–November in year 2003. Basically, the right panel is $\text{NO}^+(\text{v})$ VER averaged over the Halloween 2003 storm period. It is clear that $r > 1$ for the geomagnetically disturbed periods at high-latitudes, predominantly in the auroral oval region, and $r \sim 1$ equatorward of the auroral oval region and for geomagnetically quiet periods. The robustness of the $\text{NO}^+(\text{v})$ VER SQR at all latitudes was also demonstrated recently by Mertens et al. (2009b).

The SABER-derived $\text{NO}^+(\text{v})$ VER SQR in (1) is the key quantity for developing a storm-time correction to E-region electron densities, based on the fundamental relationships specified in (1) and (2). Once the SQR is computed, the IRI E-region electron density peak concentration can be corrected for geomagnetic activity, i.e.,

$$[NmE(t)]_{\text{Storm}}^{\text{IRI}}(\text{peak}) = \tilde{r}(\lambda_m, \varphi_m, t) \times [NmE]_{\text{Nominal}}^{\text{IRI}}(\text{peak}). \quad (3)$$

Thus, the SABER-derived $\text{NO}^+(\text{v})$ VER SQR values scale the nominal quiescent IRI E-region electron density peak, $[NmE]_{\text{Nominal}}^{\text{IRI}}(\text{peak})$, to obtain a storm-enhanced E-region electron density peak value. The SQR in (3) is given by an average over altitude:

$$\tilde{r}(\lambda_m, \varphi_m, t) = \frac{1}{\Delta z} \int_{Z_B}^{Z_T} r(z, \lambda_m, \varphi_m, t) dz. \quad (4)$$

The terms $Z_{B,T}$ represent the bottom and top altitude limits of integration, respectively, and Δz is the altitude interval. The top and bottom altitude limits in (4) are determined from our SABER/ISR SQR validation studies. Validations studies presented in Section 4 suggest that the bottom and top altitude limits of integration should be 115 km and 120 km, respectively. The physical rationale for these altitude integration limits will be discussed in a future report containing a detailed error analysis.

The SQR defined in (1) can also be expanded in terms of a geomagnetic forcing parameter (G):

$$r(z, \lambda_m, \varphi_m; t) = \sum_{i=0}^N a_i(z, \lambda_m, \varphi_m) G^i(z, \lambda_m, \varphi_m; t), \quad (5)$$

where a_i are the expansion coefficients. The geomagnetic forcing parameter represents the E-region response to a geomagnetic storm event. Therefore, it can be expressed as a convolution between an impulse response function F and a geomagnetic index D , such that

$$G(z, \lambda_m, \varphi_m; t) = \int_{-T_S}^T F(z, \lambda_m, \varphi_m; \tau) D(t - \tau) d\tau. \quad (6)$$

The upper limit of the integral above is referred to as the effective memory of the storm-time response (T) and the lower limit is the start time (T_S). Geomagnetic index parameters such as the Hemispheric Power index (HP), Disturbed Storm Time (Dst), ap index, and the Auroral Electroject (AE) index, can be considered as possible candidates for the geomagnetic index D . Once the geomagnetic index is chosen, the response function can be readily determined by

$$r(z, \lambda_m, \varphi_m; t) = \int_{-T_S}^T F(z, \lambda_m, \varphi_m; \tau) D(t - \tau) d\tau. \quad (7)$$

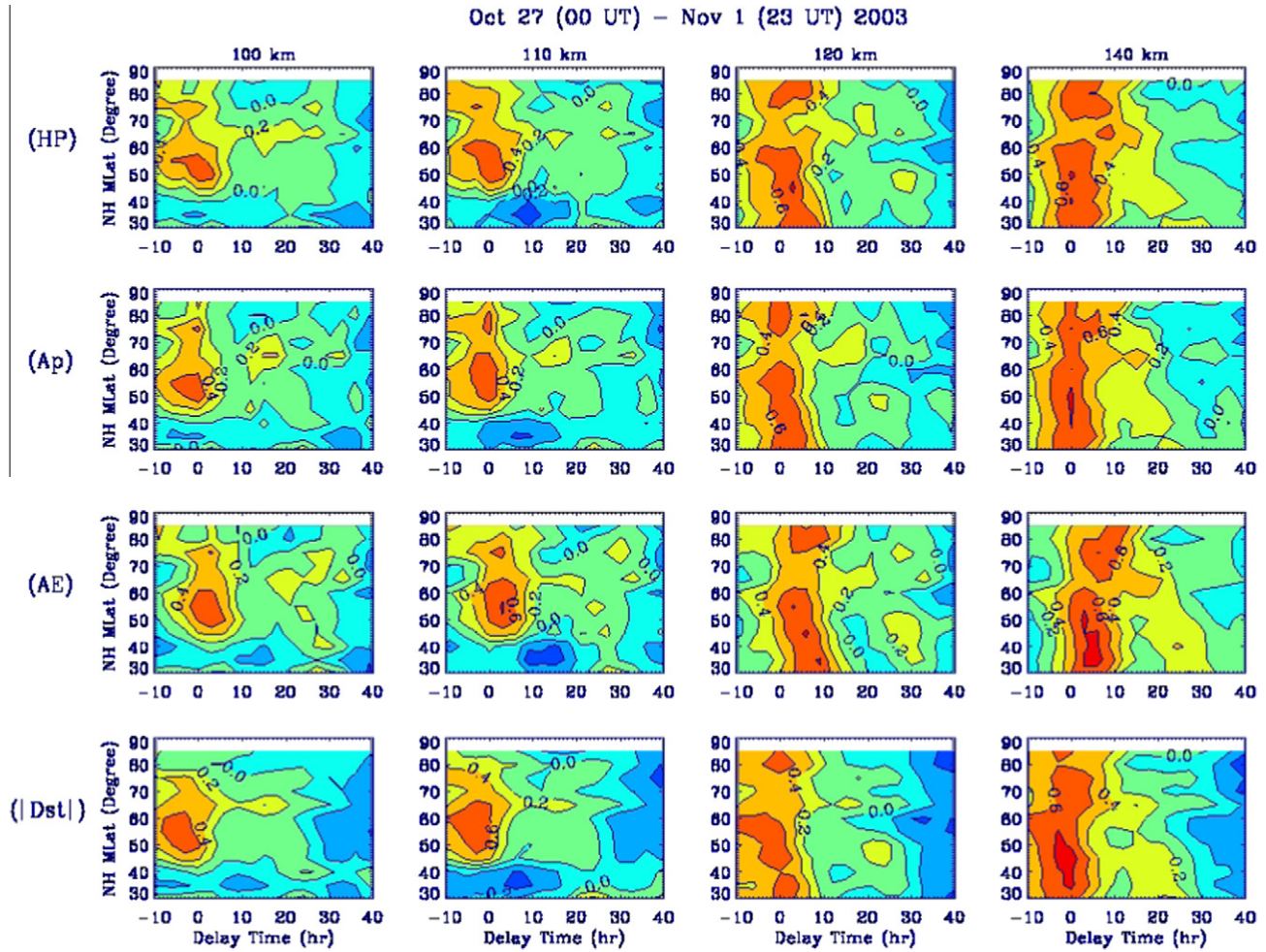


Fig. 4. Cross-correlation between $\text{NO}^+(\text{v})$ VER and HP, ap, AE, and $|\text{Dst}|$ indices for October 27 (00 UT)–November 1 (23 UT), 2003.

The above equation assumes a linear impulse–response relation between the external geomagnetic driver and the response of the E-region ionosphere, as characterized by the $\text{NO}^+(\text{v})$ VER SQR. The VER SQR quantities computed from the SABER dataset from 2002 to 2006 are used to solve for the response function in (7). The above equation can be discretized and solved by matrix inversion using standard Singular Value Decomposition (SVD) techniques (Press et al., 1992). With a known response function determined from (7), the E-region electron density storm-time enhancement at any specified geographic location and time can be derived from (5) and (6). In the next section, a cross-correlation approach is presented to determine the geomagnetic index described in (6) and (7).

3. Halloween 2003 cross-correlation analysis

In this section, SABER $\text{NO}^+(\text{v})$ VER data from the Halloween 2003 geomagnetic storm period is cross-correlated with commonly used geomagnetic indices to determine which geomagnetic driver index should be used in (6). The cross-correlation function is defined as (Vassiliadis et al., 2002)

$$C(\lambda_m, \tau) = \frac{1}{T} \frac{1}{\sigma_D \sigma_{\text{VER}}} \sum_{i=1}^T (\text{VER}(\lambda_m, t_i + \tau) - \langle \text{VER}(\lambda_m) \rangle) (D(t_i) - \langle D \rangle), \quad (8)$$

where $\langle \rangle$ denote averaged data and σ is the standard deviation. The SABER $\text{NO}^+(\text{v})$ VER data used in this analysis corresponds to 6 days during the Halloween 2003 storm event, from October 27 to November 1. The VER data were sorted and averaged into 5° magnetic latitude bins. In addition, the SABER $\text{NO}^+(\text{v})$ VER data and geomagnetic indices were sorted and averaged into 3-h UT time bins throughout the 6-day period. Fig. 4 shows results from cross-correlations between SABER $\text{NO}^+(\text{v})$ VER data and four geomagnetic indices: HP (upper panel), ap, AE, and the absolute value of Dst (bottom panel). Each column represents a different altitude: 100 km, 110 km, 120 km, and 140 km, respectively. The vertical axes represent the Northern Hemisphere (NH) magnetic latitude and the horizontal axis is the delay time (τ in (8)) in hours. The colored contours correspond to the cross-correlation.

Since the HP index is a proxy for the physical source of the E-region response, HP will be considered the benchmark index to which the other geomagnetic indices will

be compared. The broad features of the cross-correlations for each geomagnetic index separate into two distinct patterns. At 110 km and below, the peak cross-correlations are concentrated between 50° and 60° in magnetic latitude, corresponding to the auroral oval region, and have an approximate zero response time. This feature is consistent with auroral dosing followed by fast ion-neutral reactions and prompt $4.3 \mu\text{m}$ emissions (Mertens et al., 2007a,b, 2008). Above 110 km the peak cross-correlations extend to lower latitudes with a longer response time.

It is well known that heated molecular enriched air can be transported from high-latitudes to lower latitudes (Richards, 2004). The enhanced temperature and molecular densities increases the rate of production of mid-latitude NO densities, which can charge exchange with O_2^+ to produce enhanced NO^+ densities. Thus, the peak in the cross-correlation functions at low latitudes above 110 km could be due to horizontal transport of molecular oxygen. The direct transport of NO from the auroral dosing region to mid-latitudes is still an open question (Richards, 2004).

The main conclusion from Fig. 4 is that the common geomagnetic indices (ap, AE, and Dst) are comparable in magnitude and morphology to our benchmark HP index in capturing the correlation between SABER $\text{NO}^+(\text{v})$ VER and auroral particle precipitation. Slight differences in morphology are noticed at 120 km and above between the $\text{NO}^+(\text{v})$ VER response to HP and ap and the $\text{NO}^+(\text{v})$ VER response to AE and Dst. The ap index may be dominated by ground-level magnetic disturbances associated with the field-aligned currents due to enhanced conductivity from the auroral particle precipitation. Thus, the HP and ap-indices are closely associated with the same source phenomena, namely the particle precipitation. The AE and Dst indices, on the other hand, may be responding to common source phenomena in the magnetotail region, in

addition to the auroral particle precipitation. Further studies are required to understand Fig. 4 in detail.

Since the ap index is already an input into IRI, ap may be the most practical index for use in IRI. Once the geomagnetic index is chosen, the parametric relation between SABER $\text{NO}^+(\text{v})$ VER SQR and the geomagnetic index can be implemented in the correction procedure described in Section 2. Since this procedure is based on the fundamental relations in (1) and (2), it is necessary to demonstrate the feasibility of these relations. In the next section, SABER–ISR coincidences are found and the SQRs are compared.

4. SABER–ISR coincidences

In order to validate (1) and (2), SABER and ISR coincident measurements are selected during different geomagnetic storms. Quiet periods are defined by $kp < 3$. Geomagnetic active periods are defined by $kp > 4$. Nighttime data is defined such that the solar zenith angle is greater than 104° , which ensures no solar illumination below 200 km.

ISR measurements were selected from three different locations: EISCAT VHF at Tromso, Norway (69.59N , 19.23E), Loneybyen, Norway (78.15N , 16.03E), and Sondrestrom, Greenland (66.99N , 309.05E). Coincidences with SABER at each location were taken during three geomagnetic storm-time events. To define a SABER/ISR spatial coincidence, the ISR location is centered in a magnetic latitude and longitude box that is extended $\pm 2.5^\circ$ in magnetic latitude and $\pm 10^\circ$ in magnetic longitude from the ISR location. To define a SABER/ISR time coincidence, we selected a 0.1 h time difference between the SABER and ISR measurements. Each SABER measurement that fell within the magnetic box centered on the ISR locations, and fell within the selected time difference, was taken as a coincidence. ISR quiet time was taken within days prior to and

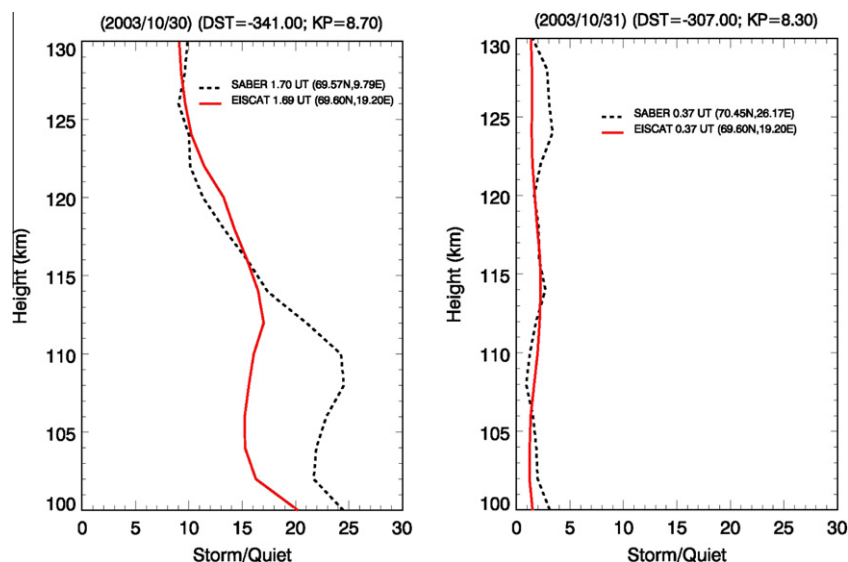


Fig. 5. EISCAT VHF and SABER $\text{NO}^+(\text{v})$ VER SQR comparisons for October 30 and October 31, 2003.

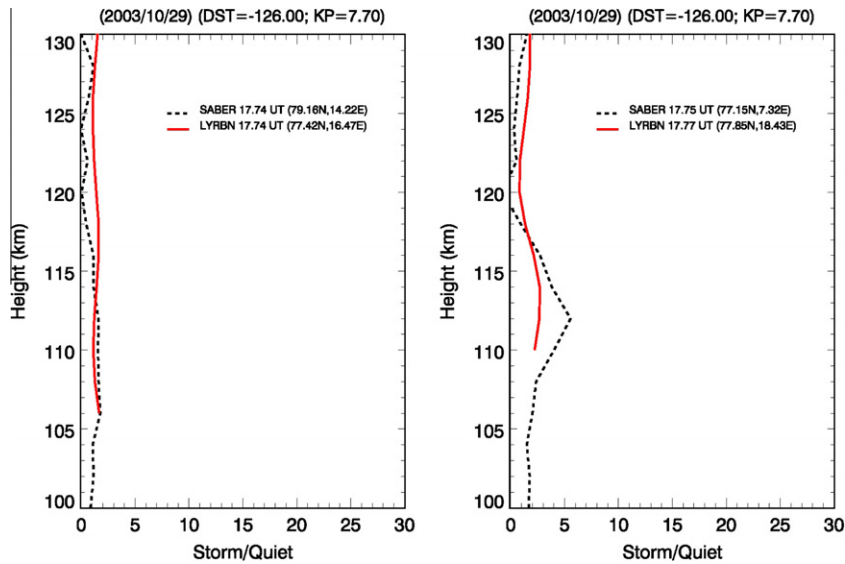


Fig. 6. SABER and Loneyarbyen SQR comparisons for October 29, 2003. The Loneyarbyen profile was constructed locations from off-vertical beam measurements.

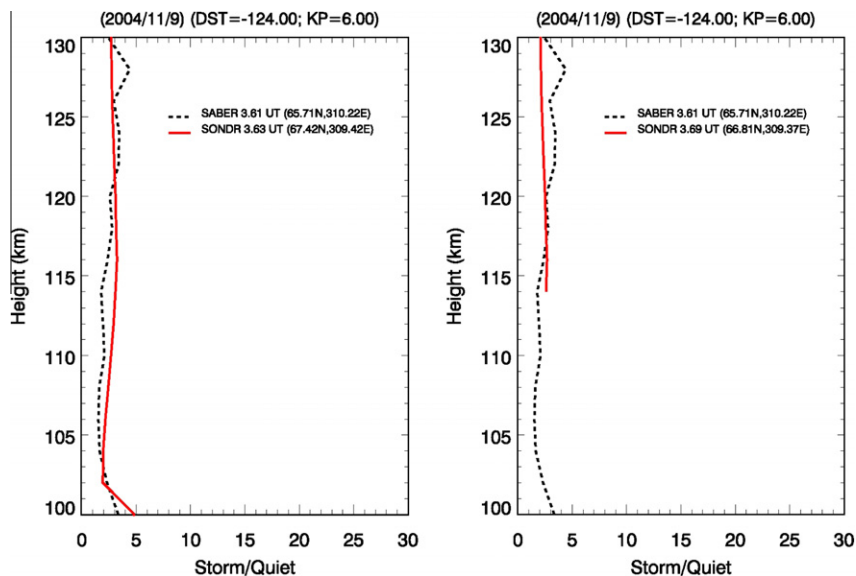


Fig. 7. SABER and Sondrestrom SQR comparisons for November 09, 2004 magnetic storm.

following each geomagnetic storm, according to the availability of the data. On the other hand, SABER quiet times were selected according to the yaw maneuvers as depicted in Fig. 1. For example, if a SABER/ISR coincidence occurred in October, SABER quiet data from the yaw period corresponding to September 19 through November 21 are averaged for all years from 2002 until 2006. Fig. 5 shows two SABER and EISCAT Tromso coincidences on October 30 (left panel) and October 31 (right panel), 2003. SABER and ISR SQR values show good agreement, especially from 114 km through 120 km. These two events occurred during the Halloween 2003 solar-geomagnetic storm events. ISR quiet data were taken from 10/06/2003 to 10/28/2003. The

spatial-temporal differences between the SABER/ISR measurements are less for the event in the right panel compared to the left, corresponding to better agreement for the event in the right panel.

Fig. 6 shows two SABER and Loneyarbyen ISR coincidences for October 29, 2003. These two scans are at the onset of the Halloween storm with kp and Dst indices lower than the previous scans shown in Fig. 5. The ISR position is located further north, at the boundary of the auroral oval. In this case, the ISR experiment was performed with off-vertical beam measurements. ISR quiet data were taken from before (10/06/2003–10/25/2003) and after (11/02/2003–11/04/2003) the geomagnetic storm

event. SABER quiet data dates were the same as in the previous case but with a different magnetic grid location. As can be seen from Fig. 6, results show similar agreement with the events in Fig. 5.

Fig. 7 shows the final case study for SABER and ISR comparisons. ISR measurements are from the Sondrestrom facility with off-vertical beam measurements. The data shown are from a November 9, 2004 geomagnetic storm. Quiet ISR data are taken from before (10/22/2004–10/29/2004) and after (11/04/2004–11/05/2004) the November 2004 storm event. Since this event corresponds to the same SABER yaw cycle as the previous events in Figs. 5 and 6, SABER quiet data are taken from the same climatological period, but with a different magnetic grid location. As clearly seen in Fig. 7, SABER/ISR SQR comparisons show remarkable agreement in both cases.

5. Conclusions

Results derived from SABER $\text{NO}^+(\nu)$ VER measurements suggest that this product can be used as an effective proxy to monitor the response of the nighttime E-region ionosphere to geomagnetic storm activity. We have demonstrated that we can derive a storm-time E-region electron density correction factor that can be directly applied to IRI. This conclusion is supported by two main results from this study. One, SABER $\text{NO}^+(\nu)$ VER SQR comparisons with ISR SQR show remarkable agreement for weak to strong geomagnetic storm activity. The SABER $\text{NO}^+(\nu)$ VER SQR is the fundamental quantity that will be used to develop a storm-time correction to E-region electron densities. Secondly, the cross-correlation studies between SABER $\text{NO}^+(\nu)$ VER and the common geomagnetic activity indices show comparable results to the benchmark SABER $\text{NO}^+(\nu)$ VER and HP index correlations. Since the HP index is indicative of the physical source responsible for the storm-time enhancements to the E-region electron density, this result indicates that the common geomagnetic indices can be used to parameterize the electron density enhancements with a simple geomagnetic driver index. Moreover, since the ap index is already an input variable in the IRI, our E-region storm model approach can be readily implemented in IRI. Our next steps will be to develop the parametric fit between storm-time SABER $\text{NO}^+(\nu)$ VER SQR and the geomagnetic activity indices, and validate our empirical storm-time E-region electron density correction with ISR measurements.

References

- Bilitza, D. International Reference Ionosphere. *Radio Sci.* 36 (2), 261–265, 2001.
- Fox, J.L., Sung, K.Y. Solar activity variations of the Venus thermosphere/ionosphere. *J. Geophys. Res.* A 106 (10), 21305–21335, 2001.
- Mertens, C.J., Mast, J.C., Winick, J.R., Russell III, J.M., Mlynczak, M.G., Evans, D.S. Ionospheric E-region response to solar-geomagnetic storms observed by TIMED/SABER and application to IRI storm-model development. *Adv. Space Res.* 39, 715–728, 2007a.
- Mertens, C.J., Winick, J.C., Russell III, J.M., Mlynczak, M.G., Evans, D.S., Bilitza, D., Xu, X. Empirical storm-time correction to the International Reference Ionosphere Model E-region electron density parameterizations using observations from TIMED/SABER, in: *Proceedings of the SPIE, Remote Sensing of Clouds and the Atmosphere XII*, vol. 6745, Florence, Italy, September 17–19, p. 67451L, 2007b.
- Mertens, C.J., Fernandez, J.R., Xu, X., Evans, D.S., Mlynczak, M.G., Russell III, J.M. A new source of auroral infrared emission observed by TIMED/SABER. *Geophys. Res. Lett.* 35, L17106, doi:10.1029/2008GL034701, 2008.
- Mertens, C.J., Winick, J.C., Picard, H., Evans, D.S., Lopez-Puertas, M., Wintersteiner, P.P., Xu, X., Mlynczak, M.G., Russell III, J.M. Influence of solar-geomagnetic disturbances on SABER measurements of 4.3 μm emission and the retrieval of kinetic temperature and carbon dioxide. *Adv. Space Res.* 43, 1325–1336, 2009a.
- Mertens, C.J., Xu, X., Fernandez, J.R., Bilitza, D., Russell III, J.M., Mlynczak, M.G. Development of a geomagnetic storm correction to the International Reference Ionosphere E-region electron densities using TIMED/SABER observations, in: *Proceedings of SPIE, Remote Sensing of Clouds and the Atmosphere XIV*, vol. 7475, Berlin, Germany, August 31–September 3, p. 747508, 2009b.
- Philips, B.L. A technique for the numerical solution of certain integral equations of the first kind. *J. ACM* 9, 84–97, 1962.
- Press, W.H., Teukolsky, S.A., Vetterling, W.T., Flannery, B.P. *Numerical Recipes in FORTRAN: The Art of Scientific Computing*. Cambridge University Press, New York, 1992.
- Richards, P.G. On the increases in nitric oxide density at midlatitudes during ionospheric storms. *J. Geophys. Res.* 109, A06304, doi:10.1029/2003JA010110, 2004.
- Russell III, J.M., Mlynczak, M.G., Gordley, L.L., Tansok, J., Esplin, R. An overview of the SABER experiment and preliminary calibration results, in: *Proceedings of the SPIE, 44th Annual Meeting, Denver, Colorado, July 18–23*, vol. 3756, pp. 277–288, 1999.
- Tikhonov, A.N. On the solution of incorrectly stated problems and the method of regularization. *Dokl. Akad. Nauk SSSR* 151, 501–504, 1963.
- Torr, M.R., Torr, D.G., Richards, P.G., Yung, S.P. Mid- and low-latitude model of thermospheric emissions I. $\text{O}^+(\text{}^2\text{P})$ 7320 Å and $\text{N}_2(\text{}^2\text{P})$ 3371 Å. *J. Geophys. Res.* A 95 (12), 21147–21168, 1990.
- Twomey, S. On the numerical solution of Fredholm integral equations of the first kind by the inversion of the linear system produced by quadrature. *J. Assoc. Comput.* 10, 97–101, 1963.
- Twomey, S. *Introduction to the Mathematics of Inversion of Remote Sensing and Indirect Measurements*. Elsevier, New York, 1977.
- Vassiliadis, D., Klimas, A.J., Kanekal, S.G., Baker, D.N., Weigel, R.S. Long-term average, solar cycle, and seasonal response of magnetospheric energetic electrons to the solar wind speed. *J. Geophys. Res.* 107 (A11), 1383, doi:10.1029/2001JA000506, 2002.